Multibody Syst Dyn (2020) 48:427–450
https://doi.org/10.1007/s11044-019-09702-3

Motion of a disk in contact with a parametric 2D curve and Painlevé's paradox

Flavius Portella Ribas Martins[1] ·
Agenor de Toledo Fleury[1] · **Flavio Celso Trigo**[1]

Received: 26 December 2018 / Accepted: 9 September 2019 / Published online: 18 September 2019

Abstract This paper addresses the modeling and simulation of a homogeneous disk that undergoes plane motion constrained to be in permanent contact with and in the same plane as a two-dimensional curve described by a parametric equation. Except for the elementary cases in which the curve is a straight line or an arc of circumference, the investigated problem presents significant challenges to both modeling and simulation. In addition to the necessity of using differential geometry methods to calculate local geometrical properties of the motion, this system exhibits typical difficulties of non-smooth dynamics. Different modes of operation require the synthesis of suitable rules for switching systems of differential equations and, due to the discontinuities caused by the exchange of dynamic models, numerical integration methods suitable for solving stiff problems are necessary. It should also be emphasized that the dynamic model here developed shows the Painlevé's paradox, caused by the application of a simplified law of friction (Coulomb's law) to a rigid body subjected to an unilateral constraint. Among the results obtained in this work, we would like to highlight the following: (i) the realization that both the geometry of the contact curve and that followed by the center of mass of the disk must be considered to construct a correct dynamic model for the motion; (ii) a detailed procedure to identify the instant the disk stops sliding and initiates a pure rolling motion on the two-dimensional track represented by a $\mathfrak{C}_2$ class curve C in parametric form; (iii) the realization that, for arbitrary geometries of flat two-dimensional curves of class $\mathfrak{C}_2$ and simplified models of friction, it is not possible to establish an arbitrary initial kinematic condition (a necessity for integrating the equations of motion) without incurring in a paradoxical result, known in the literature as Painlévé's paradox. We consider that the approach adopted in this work might contribute to building dynamic models of hybrid systems, especially those with non-elementary geometric characteristics.

Keywords Non-smooth dynamical systems · Hybrid dynamical systems · Painlevé's Paradox · Impact with friction

✉ F.C. Trigo
trigo.flavio@usp.br

[1] University of Sao Paulo, Sao Paulo, Brazil

1 Introduction

The plane motion of a disk that rolls and slides in contact with a curve, be it a horizontal or an inclined straight line, or still an arc of a circumference, is a classic problem of rigid-body dynamics quite present in textbooks adopted in undergraduate engineering courses [1, 11] as well as in articles of Physics education journals [6, 19, 20]. Due to the plane motion constraint and the simplicity of the geometry of those curves, it is possible to adopt an algebraic approach to finding a solution to these problems, but considering a given instant of the motion, not its evolution over time. In this case, Newton's and Euler's equations, combined with the friction laws, are solved altogether to determine the reaction forces, the acceleration of the center of mass and the disk angular acceleration at a given instant.

As there is a consensus that the plane motion of a disk in contact with a straight line or an arc of a circle is a completely solved problem, simulation and analysis of these movements has been rarely approached in recent scientific articles. On the other hand, the classic three-dimensional motion of a disk that rolls and slides on a flat surface, continues to be the subject of numerous scientific articles, since, for this problem, the trajectories in the phase space exhibit quite complex geometry, which provokes interesting discussions in the field of nonlinear dynamics. In the following paragraphs of this section, we will present a brief summary of some articles that investigated the dynamics of the 3D movement of a disc in contact with a flat surface.

An article by [12] addresses the integrability of the equations of motion of the disk. The analysis encompasses both the rolling and the sliding motions, but in a exclusive way (*i.e.*, it is either supposed that friction forces act and the disk rolls without slipping, or that friction forces are negligible and the disk slides). Simulations of the mathematical models generated the necessary data for the construction of the bifurcation diagrams, which were then found to be of two types—saddle-node and pitchfork.

The chaotic phenomena exhibited by the phase space trajectories representing the dynamics of the motion of the disk were also investigated in the article of [2], but these authors considered only the case of pure rolling motion. Contrary to results previously accepted in the literature as true, these authors have proved through simulations that, for almost all initial conditions compatible with pure rolling motion, the trajectories described by the point of contact of the disk with the surface are bounded.

The same problem was studied by [16], who used a law of friction that interpolates between the laws of dry and viscous friction; this greatly facilitated the numerical implementation of the dynamics equations. The authors perform a rigorous mathematical analysis, with the intention of identifying the initial conditions of the movement that produce stationary solutions as well as the ranges of variation compatible with the stability of these solutions.

The movement of the disk was experimentally investigated using computer vision techniques [13]. From the sequences of images taken by a video camera, and using Fourier analysis, the temporal evolution of the angles of precession ψ, nutation θ, and spin ϕ of the disk were estimated for different initial values of ψ, θ, ϕ, determined analytically in order to satisfy the pure rolling motion condition. These experiments showed that, in fact, no sliding of the disk was observed while the nutation angle was smaller than $\simeq 80^\circ$. The authors thus concluded that the rolling friction is primarily responsible for the loss of energy in the early stages of the disk movement.

The 3D motion of the disk was thoroughly studied by [8]. The computational model developed by these authors predicts the possibility of occurrence of multiple transitions between the two characteristic modes of movement of the disk—sliding and pure rolling motion. Although the mathematical model is based on the rigid-body hypothesis, the authors

conjecture that the large variations of magnitude of the normal force observed during the final stage of the simulations would be related to events of contact loss and the occurrence of impulses which would give rise to the characteristic increase in the audible frequency of the sound during the final phase of the disk movement.

It is important to stress that the above-mentioned articles, with the exception of [8], analyse either the rolling or the sliding movements of the disk. Such approaches are suitable for investigating problems in nonlinear dynamics, encompassing all the questions related to the geometry of the phase space, but prevents the discussion of the important problem of non-smooth dynamics, concerning the identification of the instant of transition between the modes of motion.

In the present article, we will explore, with the aid of numerical simulations, the dynamics of a homogeneous rigid disk undergoing plane motion constrained to maintain contact with a generic two-dimensional curve C represented in parametric form; in addition, the disk never quits the plane of the bi-dimensional curve. Despite its apparent simplicity, such a problem presents unexpected modeling and simulation challenges, unless the curve is a straight line or an arc of circumference; those aspects, to the knowledge of the authors, have not yet been explored in the literature.

The paper is organized as follows: In Sect. 2, the geometry of the contact curve is described using curvilinear coordinates. In Sect. 3 the Lagrange equations are used to build the disk dynamical model in its two modes of operation. The state-space model of the disk is presented in Sect. 4. The inherent simulation difficulties are stressed and solutions to overcome them are proposed in Sect. 5. Sections 6 and 7, respectively, display the simulation results and conclusions of the work.

2 Description of the track and its geometric properties

Considering the curvilinear abscissa S as a parameter, a curve C_C, Fig. 1, can be represented as

$$(C - O) = \mathbf{r}(S) = f_x(S)\mathbf{i} + f_y(S)\mathbf{j}. \tag{1}$$

Once the class C_2 functions $f_x(S)$ and $f_y(S)$ are known, the geometric properties of C_C can be immediately determined. So, the unit local tangent and normal vectors, $\mathbf{T}$ and $\mathbf{N}$, are given, respectively, by

$$\mathbf{T}(S) = \frac{\mathbf{r}'(S)}{|\mathbf{r}'(S)|} = \frac{f_x'(S)}{(f_x'^2 + f_y'^2)^{1/2}}\mathbf{i} + \frac{f_y'(S)}{(f_x'^2 + f_y'^2)^{1/2}}\mathbf{j}, \tag{2}$$

$$\mathbf{N}(S) = \mathbf{k} \wedge \mathbf{T}(S) = -\frac{f_y'(S)}{(f_x'^2 + f_y'^2)^{1/2}}\mathbf{i} + \frac{f_x'(S)}{(f_x'^2 + f_y'^2)^{1/2}}\mathbf{j}, \tag{3}$$

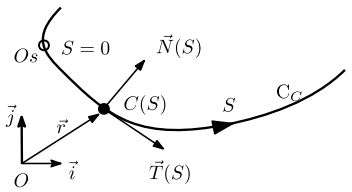

Fig. 1 Two-dimensional curve track

and the local radius of curvature P is calculated from

$$P(S) = \frac{[|\mathbf{r}'(S)|^2]^{3/2}}{|\mathbf{r}'(S) \wedge \mathbf{r}''(S)|} = \frac{[f_x'^2(S) + f_y'^2]^{3/2}}{|f_x'(S) f_y''(S) - f_y'(S) f_x''(S)|}. \tag{4}$$

In Eqs. (2)–(4), the apostrophe means derivation with respect to S, e.g., $f_x' = df_x/dS$. Moreover, we will assume hereafter that $P(S)$ is always larger than the radius R of the disc that moves in contact with C_C.

3 Dynamics modeling

In order to build the mathematical model of the dynamics of a disk constrained to keep contact with a plane curve, we will consider the two types of motion that are compatible with such constraints: (1) sliding motion (two degrees of freedom); (2) pure rolling motion (1 degree of freedom). Those motions or modes, are governed by distinct sets of differential equations and the sudden transition from sliding motion (mode 1) to a pure rolling one (mode 2) is a major issue in non-smooth hybrid dynamics systems [9] that must be addressed to tackle this problem.

3.1 Mode 1 dynamics

For the description of the kinematics of the disk, we will consider two snapshots of its movement, as shown in Fig. 2 (as stressed before, the disk and the two dimensional curve belong to the same plane during the motion considered in this article).

The disk has two degrees of freedom and its configuration can be completely determined by the following generalized coordinates: θ, the angular displacement of a material point D of the disk that, at time $t = 0$, was in contact with the curve C_C, and a time t is in a position $D(t)$ such that the angle $D(0)\hat{G}D(t)$ equals θ; s, the curvilinear abscissa of the center of mass G, measured along the curve C_G followed by G over time.

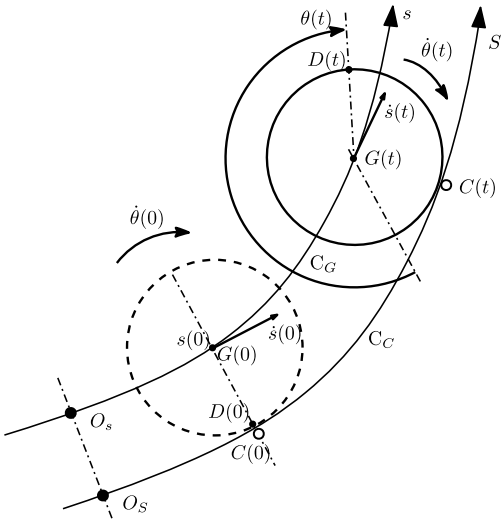

Fig. 2 Two snapshots of the disk in mode 1

It is important to stress that the curve C_G must be previously generated through a numerical offset operation applied to C_C [7], *i.e.*, for each abscissa S measured along C_C, the corresponding position of G is given by

$$G(S) = C(S) \pm R\mathbf{n}(S) \tag{5}$$

where the *plus* signal applies if the geometric contact point C lies in a concave region of the curve C_C and the *minus* sign otherwise. One must emphasize that, unless we are dealing with a straight line or a circumference, the offset and its progenitor curve do not share the same algebraic form, *i.e.*, a polynomial offset curve is not a polynomial curve; the same occurs with rational curves and even splines [14].

Considering the above discussion, we conclude that, to describe the position of G in terms of the curvilinear abscissa s, measured along C_G from a reference point O_s of C_G, it will be necessary to apply a numerical algorithm to evaluate

$$s = \int_{O_s}^{G(S)} \left|\mathbf{G}'(S)\right| dS \tag{6}$$

even in the cases where the disk moves in contact with a curve C_C described by an algebraic expression. Numerical methods must also be applied to determine all the other local geometric properties of C_G, like the radius of curvature ρ and the tangent and normal unit vectors $\boldsymbol{\tau}$ and $\mathbf{n}$. Thus, a new set of equations, similar to Eqs. (1)–(4), can be derived for the offset curve C_G:

$$(G - O) = \mathbf{r}(s) = g_x(s)\mathbf{i} + g_y(s)\mathbf{j}, \tag{7}$$

$$\boldsymbol{\tau}(s) = \frac{g_x'(s)}{(g_x'^2 + g_y'^2)^{1/2}}\mathbf{i} + \frac{g_y'(s)}{(g_x'^2 + g_y'^2)^{1/2}}\mathbf{j}, \tag{8}$$

$$\mathbf{n}(s) = \mathbf{k} \wedge \mathbf{T}(s) = -\frac{g_y'(s)}{(g_x'^2 + g_y'^2)^{1/2}}\mathbf{i} + \frac{g_x'(s)}{(g_x'^2 + g_y'^2)^{1/2}}\mathbf{j}, \tag{9}$$

and the local radius ρ of curvature is calculated from

$$\rho(s) = \frac{[g_x'^2(s) + g_y'^2]^{3/2}}{|g_x'(s)g_y''(s) - g_y'(s)g_x''(s)|}. \tag{10}$$

For a possible kinematic state given by $v_G = \dot{s}$ and $\omega = \dot{\theta}$, the free-body diagram of Fig. 3 will be considered for writing the motion equations of a disk in permanent contact with a curve C_C, under the action of gravity, the sliding friction force F and the rolling resistance, described in a simplified way by a couple M.

At any instant t, the friction force and the rolling couple are given, respectively, by

$$\mathbf{F} = -\mu N \cdot \text{sign}(\dot{s})\mathbf{T} \tag{11}$$

and

$$\mathbf{M} = -\mu_r N \cdot \text{sign}(\dot{\theta})\mathbf{k} \tag{12}$$

where μ and μ_r are the sliding and rolling friction coefficients between the disk and the track, $\mathbf{N}$ is the normal component of the contact force at time t and $\text{sign}(x)$ is a function that evaluates to -1 if $x < 0$ and to $+1$ if $x > 0$.

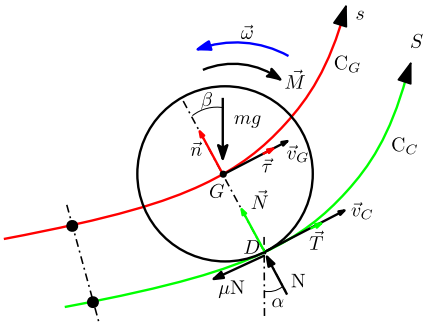

Fig. 3 Disk rolling and sliding on a curve

At this point, it is important to highlight the following mathematical difficulty we must overcome: disk kinematics can be completely determined by the state variables s, $\dot{s}$, θ, $\dot{\theta}$, but their time evolution depends on the geometric characteristics of both the curves C_C and C_G and on the kinematics of both the center of mass G and the contact point D between the disk and the curve C_C at time t (see Fig. 2).

In order to simplify the problem, we will admit that, using Eqs. (5), (6) and proper numerical methods, a function

$$s = s(S) \tag{13}$$

relating the curvilinear abscissae measured along curves C_G and C_C, can be obtained. The foregoing considerations will be used to calculate the forces and moments applied to the disk at time t. The normal component of the contact force is given by

$$N(t) = mg\cos\big(\alpha\big(S\big(s(t)\big)\big)\big) + ma_n\big(S\big(s(t)\big), \dot{S}\big(s(t)\big)\big), \tag{14}$$

where $s(t)$, the curvilinear abscissa of G, known at time t, is an input data to Eq. (13) necessary to compute the corresponding abscissa $S(t)$ of the contact point D. Next, using $S(t)$ as input, we obtain $\alpha(S(t))$, the angle between the local normal at C_C and the vertical, from the equation

$$\alpha(S) = \cos^{-1}\big(\mathbf{N}(S)\cdot\mathbf{j}\big) \tag{15}$$

where $\mathbf{N}(S)$ is given by Eq. (3).

As the disk slides on the track, the speed $\dot{S}$ of the material point D in contact with curve, as shown in Fig. 4, is

$$\dot{S} = |\mathbf{v}_D| = \big|\mathbf{v}_G + \omega\mathbf{k}\wedge(D-G)\big| = \big|\dot{s}\boldsymbol{\tau} + \dot{\theta}\mathbf{k}\wedge(D-G)\big| = \dot{s} + \dot{\theta}R. \tag{16}$$

Finally, the normal acceleration of the contact point D is

$$a_n = \frac{\dot{S}^2}{P(S)} \tag{17}$$

with $P(S)$ given by Eq. (4).

Considering the instantaneous motion shown in Fig. 4, the kinetic energy of the disk is expressed by

$$T = \frac{1}{2}mv_G^2 + \frac{1}{2}J_{Gz}\omega^2 = \frac{1}{2}m\dot{s}^2 + \frac{1}{2}J_{Gz}\dot{\theta}^2. \tag{18}$$

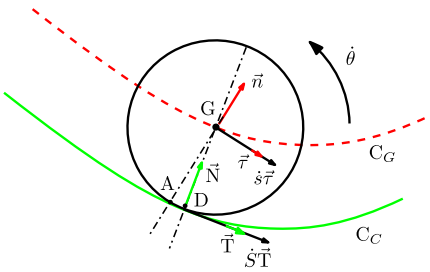

Fig. 4 Velocities of the disk in mode 1

The virtual power $\delta\mathfrak{P}$ of the forces acting on the disk in an admissible field of virtual velocities is

$$\delta\mathfrak{P} = -mg\mathbf{j}\cdot\frac{\delta\mathbf{G}(s)}{dt} - \mu N(S)\cdot\operatorname{sign}(\dot{S})\mathbf{T}\cdot\frac{\delta S}{dt}\mathbf{T} - \mu_r N(S)\cdot\operatorname{sign}(\dot{\theta})\frac{\delta\theta}{dt},$$

and, since $\delta\mathbf{G}(s)/dt = \dot{s}\boldsymbol{\tau}$ and $\delta\theta/dt = \dot{\theta}$, the above expression becomes

$$\delta\mathfrak{P} = -mg\mathbf{j}\cdot\dot{s}\boldsymbol{\tau} - \mu N\operatorname{sign}(\dot{S})\dot{S} - \mu_r N\operatorname{sign}(\dot{\theta})\dot{\theta}. \tag{19}$$

Defining

$$\Gamma_1 = g\cos\big(\alpha\big(S(s)\big)\big) + \frac{(\dot{s}+R\dot{\theta})^2}{P(S(s))} \tag{20}$$

and introducing Eqs. (14)–(16) into Eq. (19) one obtains

$$\begin{aligned}\delta\mathfrak{P} = &-m\big[g\sin\big(\beta(s)\big) + \mu\Gamma_1\operatorname{sign}(\dot{s}+R\dot{\theta})\big]\dot{s}\\ &- m\Gamma_1\big[\mu R\operatorname{sign}(\dot{s}+R\dot{\theta}) + \mu_r\operatorname{sign}(\dot{\theta})\big]\dot{\theta}\end{aligned} \tag{21}$$

where $\beta(s)$ is given by

$$\beta(s) = \cos^{-1}\big(\mathbf{n}(s)\cdot\mathbf{j}\big). \tag{22}$$

Examining Eq. (21), we conclude that the generalized forces F_s and F_θ are, respectively,

$$F_s = -m\big[g\sin\big(\beta(s)\big) + \mu\Gamma_1\operatorname{sign}(\dot{s}+R\dot{\theta})\big], \tag{23}$$

$$F_\theta = -m\Gamma_1\big[\mu R\operatorname{sign}(\dot{s}+R\dot{\theta}) + \mu_r\operatorname{sign}(\dot{\theta})\big]. \tag{24}$$

At this point we have all the elements to apply the Lagrangian equations for the generalized coordinates s and θ, *i.e.*,

$$\frac{d}{dt}\left(\frac{\partial T}{\partial\dot{s}}\right) - \frac{\partial T}{\partial s} = F_s, \tag{25}$$

$$\frac{d}{dt}\left(\frac{\partial T}{\partial\dot{\theta}}\right) - \frac{\partial T}{\partial\theta} = F_\theta. \tag{26}$$

Thus, we obtain the following second-order differential equations:

$$\ddot{s} = -\big[g\sin\big(\beta\big(S(s)\big)\big) + \mu\Gamma_1\operatorname{sign}(\dot{s}+R\dot{\theta})\big], \tag{27}$$

$$\ddot{\theta} = -\frac{m}{J_{Gz}} \Gamma_1 \left[\mu R \, \mathrm{sign}(\dot{s} + R\dot{\theta}) + \mu_r \, \mathrm{sign}(\dot{\theta}) \right], \tag{28}$$

where Γ_1 and $\beta(s)$ are given, respectively, by Eqs. (20) and (22).

It is important to stress that the differential Eqs. (27)–(28) describe exclusively the motion of the disk in mode 1. They are valid only while the normal contact force is positive, such that

$$\Gamma_1 = g \cos\big(\alpha\big(S(s)\big)\big) + \frac{(\dot{s} + R\dot{\theta})^2}{P(S(s))} > 0 \tag{29}$$

and the sliding speed of the disk is incompatible with pure rolling motion, *i.e.*:

$$|\mathbf{v}_D| = \dot{s} + R\dot{\theta} \neq 0. \tag{30}$$

From the instant that inequality of Eq. (30) no longer holds, the disk performs a free motion (mode 3) for which the differential equations

$$\begin{aligned} \ddot{z} &= -g, \\ \ddot{\theta} &= 0, \end{aligned} \tag{31}$$

and the constraints

$$F = N = 0 \tag{32}$$

represent the new dynamic model of the disk.

On the other hand, as long as the holonomous constraint

$$\dot{s} + R\dot{\theta} = 0 \tag{33}$$

is suddenly introduced, the disk loses one degree of freedom (s) and initiates a pure rolling motion (mode 2) for which the coordinate θ, alone, is sufficient to describe its configuration.

3.2 Dynamical model of a disk in mode 2

During this phase of the motion, the tangential contact force between the disk and the track satisfies the inequality

$$\big|\mathbf{F}(t)\big| < \mu \big|\mathbf{N}(t)\big| \tag{34}$$

and the material point D of the disk in contact with C_C coincides with I, the instantaneous center of rotation of the disk (see Fig. 5); so, it has null velocity at this instant. In such circumstances, the kinetic energy is given by

$$T = \frac{1}{2} J_{Iz} \dot{\theta}^2 = \frac{1}{2} \big(J_{Gz} + mR^2\big) \dot{\theta}^2 \tag{35}$$

and the virtual power $\delta\mathfrak{P}$ of the forces acting on the disk in an admissible field of virtual velocities is

$$\delta\mathfrak{P} = -mg\mathbf{j} \cdot \frac{\delta \mathbf{G}(s)}{dt} - \mu_r N(S) \cdot \mathrm{sign}(\dot{\theta}) \frac{\delta\theta}{dt}.$$

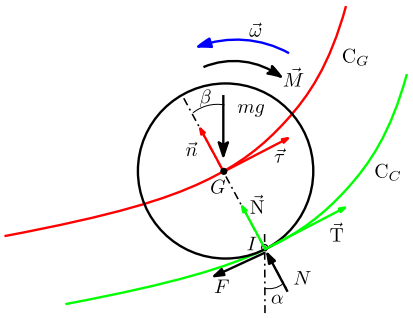

Fig. 5 Disk rolling without sliding on a plane curve

Considering that s is no more a generalized coordinate, but a dependent variable satisfying holonomous constraint of Eq. (33), we write

$$\frac{\delta \mathbf{G}(s)}{dt} = \dot{s}\boldsymbol{\tau} = -\dot{\theta} R \boldsymbol{\tau}.$$

Noticing, moreover, that the speed of instant center I is

$$|\mathbf{v}_I| = \dot{S} = \dot{\theta} R,$$

and defining

$$\Gamma_2 = g\cos\big(\alpha(R\theta)\big) + \frac{\dot{\theta}^2 R^2}{P(R\theta)}, \tag{36}$$

with $P(R\theta)$ and $\alpha(r\theta)$ given, respectively, by Eqs. (4) and (15), the expression of the virtual power becomes

$$\delta\mathfrak{P} = -mg\mathbf{j}\cdot(-\dot{\theta} R)\boldsymbol{\tau} - \mu_r m \Gamma_2 \operatorname{sign}(\dot{\theta})\dot{\theta}. \tag{37}$$

Introducing Eqs. (14)–(15) into Eq. (37) one finally obtains

$$\delta\mathfrak{P} = \big[mgR\sin\beta(R\theta) - \mu_r m \Gamma_2 \operatorname{sign}(\dot{\theta})\big]\dot{\theta}, \tag{38}$$

with $\beta(R\theta)$ given by Eq. (22). From Eq. (38) the generalized force F_θ immediately follows:

$$F_\theta = mgR\sin\beta(R\theta) - \mu_r m \Gamma_2 \operatorname{sign}(\dot{\theta}). \tag{39}$$

Using Eqs. (35) and (39) in the Lagrange equation for coordinate θ (Eq. (26)), we arrive at the second-order differential equation that rules mode 2:

$$\ddot{\theta} = -\frac{m}{J_{Gz} + mR^2}\big[gR\sin\beta(R\theta) + \mu_r \Gamma_2 \operatorname{sign}(\dot{\theta})\big] \tag{40}$$

where $P(R\theta)$, $\alpha(R\theta)$, and $\beta(R\theta)$ are, respectively, given by Eqs. (4), (15), and (22).

4 State-space variables

In order to apply the numerical methods of integration, the second-order differential Eqs. (27)–(28) and (40) are represented in a state-space form. For mode 1, the state-space

equations are

$$\begin{aligned}
\frac{ds}{dt} &= v_s, \\
\frac{dv_s}{dt} &= -g\sin\big(\beta\big(S(s)\big)\big) - \mu\Gamma_1\,\mathrm{sign}(v_s + R\omega), \\
\frac{d\theta}{dt} &= \omega, \\
\frac{d\omega}{dt} &= -\frac{m}{J_{Gz}}\Gamma_1\big[\mu R\,\mathrm{sign}(v_s + R\omega) + \mu_r\,\mathrm{sign}(\omega)\big],
\end{aligned} \tag{41}$$

whereas mode 2 is described by the first-order equations shown:

$$\begin{aligned}
\frac{d\theta}{dt} &= \omega, \\
\frac{d\omega}{dt} &= -\frac{m}{J_{Gz} + mR^2}\big\{gR\sin\beta(R\theta) + \mu_r\Gamma_2\,\mathrm{sign}(\omega)\big\}.
\end{aligned} \tag{42}$$

Therefore, ignoring the case of contact loss, simulating the plane motion of a disk that is permanently in contact with a class C_2 two-dimensional curve of generic shape and in the same plane of this curve requires the integration of one of the two systems of first-order differential equations, (41) or (42), depending on whether the constraint of Eq. (33) is satisfied or not.

5 Simulation issues

Besides the challenges faced to build this dynamic model, the simulation of these equations is also not free of difficulties, which we classify into three categories: (1st.) geometry of the curves; (2nd.) mode switching; (3rd.) feasible initial kinematic states.

5.1 Calculating geometrical properties of the curves

The geometry of curve C_C is of major concern. We could arbitrarily increase the degree of difficulty of the problem by choosing a curve with complicate geometry, but such an approach would not contribute to the identification of the essential geometric problems that must be solved during the simulation. Thus, from this point onwards, we will admit that the disc moves in contact with a well-known curve—a convex function defined by the equation

$$y = \frac{1}{2p}x^2 \tag{43}$$

with $p \in \mathrm{R}$, $p > 0$, as shown in Fig. 6.

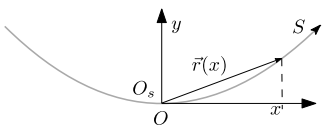

Fig. 6 Curve used in the simulations

In vector parametric form, this equation can be written as

$$\mathbf{r}(x) = f_x\mathbf{i} + f_y\mathbf{j} = x\mathbf{i} + \frac{1}{2p}x^2\mathbf{j}. \tag{44}$$

For this particular curve, all the relevant geometric properties can be determined from the value of the Cartesian abscissa x. Since

$$\lim_{|\Delta\mathbf{r}|\to 0} \Delta S/|\Delta R| = 1,$$

we can write

$$\frac{dS}{dx} = \pm\left|\frac{d\mathbf{r}}{dx}\right| = \pm\sqrt{f_x'^2 + f_y'^2} = \pm\sqrt{1 + \left(\frac{x}{p}\right)^2} = \pm\frac{\sqrt{x^2+p^2}}{p} \tag{45}$$

where the sign + must be used if $x > 0$ and − if $x < 0$.

Through the integration of Eq. (45), we obtain the curvilinear abscissa S as a function of the parameter x, *i.e.*,

$$S = \pm\int_0^x \frac{\sqrt{x^2+p^2}}{p}\,dx \tag{46}$$

where the origins O of (x, y) and O_S of S coincide, as shown in Fig. 6.

Unit tangent and normal vectors are given, respectively, by

$$\mathbf{T}(x) = \frac{p}{\sqrt{x^2+p^2}}\mathbf{i} + \frac{x}{\sqrt{x^2+p^2}}\mathbf{j}, \tag{47}$$

$$\mathbf{N}(x) = -\frac{x}{\sqrt{x^2+p^2}}\mathbf{i} + \frac{p}{\sqrt{x^2+p^2}}\mathbf{j}, \tag{48}$$

the radius of curvature P is

$$P(x) = p\left[\frac{x^2+p^2}{p^2}\right]^{3/2} = \frac{(x^2+p^2)^{3/2}}{p^2} \tag{49}$$

and the angle α between the vertical and the local tangent to the curve is obtained from

$$\alpha(x) = \cos^{-1}\big(\mathbf{T}(x)\cdot\mathbf{i}\big) = \cos^{-1}\left(\frac{p}{\sqrt{x^2+p^2}}\right) \tag{50}$$

Since the geometric properties of the parabola (Eqs. (44)–(50)) are parametrized in terms of x and not in terms of the curvilinear abscissa S, as required by the generic dynamic model synthesized for all kinds of two-dimensional curves (Eqs. (41)–(42)), we suggest the algorithm of Table 1 to obtain the required properties.

As discussed in Sect. 3.1, the locus of the center of mass G of the disk is a curve C_G generated from C_C through an offset operation (Eq. (5)). In the case of a parabola described

Table 1 Algorithm for calculating local geometric properties of the curve C_C during the simulation

1. Along the range $[x_{\min}, x_{\max}]$, apply a quadrature algorithm to evaluate Eq. (46) and construct the table $S_i = S_i(x_i)$.
2. Construct the inverse table $x_i = x_i(S_i)$.
3. During the simulation, whenever necessary, interpolate $x_i = x_i(S_i)$ in order to calculate the abscissa $\bar{x}$ corresponding to the current curvilinear abscissa $\bar{S}$.
4. With $\bar{x}$ obtained in step 3 apply Eqs. (49)–(50) to calculate the radius of curvature $P(\bar{x})$ and the angle $\alpha(\bar{x})$.

Table 2 Algorithm for calculating local geometric properties of the curve C_G

1. for each point $C(x_i, y_i)$ of C_C determine the corresponding point $G(x_i, y_i)$ of C_C using Eq. (5).
2. Along the range $[x_{\min}, x_{\max}]$, estimate the curvilinear abscissa s for each x as
   $s_j = 0, \quad \text{if } j = 0,$
   $s_j = \sum_{i=2}^{j} \sqrt{(x_i - x_{i-1})^2 + (y_i - y_{i-1})^2} \quad \text{if } j > i.$
3. Construct the tables $s_i = s_i(x_i)$, $s_i = s_i(y(x_i))$, $x_i = x_i(s_i)$, and $y_i = y_i(s_i)$.
4. Using the set of points $G(x_i, y_i)$ obtained in step 1 and the tables $x_i = x_i(s_i)$ and $y_i = y_i(s_i)$ obtained in step 3, build the partial derivative tables $g'_x(s_i) = \frac{\partial G(s_i)}{\partial x} \approx \frac{s_i - s_{i-1}}{x_i - x_{i-1}}$, $g'_y(s_i) = \frac{\partial G(s_i)}{\partial y} \approx \frac{s_i - s_{i-1}}{y_i - y_{i-1}}$, $g''_x(s_i) = \frac{dg'_x(s_i)}{ds} \approx \frac{g'_x(s_i) - g'_x(s_{i-1})}{s_i - s_{i-1}}$, and $g''_y(s_i) = \frac{dg'_y(s_i)}{ds} \approx \frac{g'_y(s_i) - g'_y(s_{i-1})}{s_i - s_{i-1}}$.
5. Use the tables $g'_x(s_i)$ and $g'_y(s_i)$ to build the vector function tables $\mathbf{n} = \mathbf{n}(s_i)$, Eq. (9).
6. Use the functions $g'_x(s_i)$, $g'_y(s_i)$, $g''_x(s_i)$, and $g''_y(s_i)$ to build the function $\rho = \rho(s)$, Eq. (10).
7. Use the function $\mathbf{n} = \mathbf{n}(s_i)$ and Eq. (22) to determine the function $\beta = \beta(s)$.

by Eq. (43), this offset curve has a closed implicit equation [17] given by

$$
\begin{aligned}
&-y^2 + \frac{16R^2}{p}x^2y^2 - \frac{4R^2}{p}x^2y + R^2 + \frac{10R^2}{p}x^2 - \frac{16}{p}x^2y \\
&- \frac{24R^4}{p}x^2 + 8R^2y^2 + \frac{1}{p}x^2y - 8R^2y + \frac{12R^2}{p^2} - 4x^4y^2 \\
&+ \frac{10}{p^2}x^4y + \frac{16}{p}x^2y^3 - 16R^4y^2 - 32R^4y + \frac{16R^2}{(\sqrt{2p})^3} \\
&- \frac{1}{4p^2}x^4 + 8R^4 + 8y^3 - \frac{2}{p^3}x^6 + 16R^6 - 16y^4 = 0.
\end{aligned} \tag{51}
$$

However, since this equation has a rather cumbersome form, it is easier to obtain the geometric properties of C_G using a numerical approach based on Eqs. (5)–(6) as suggested

Fig. 7 Plot of $S = S(s)$

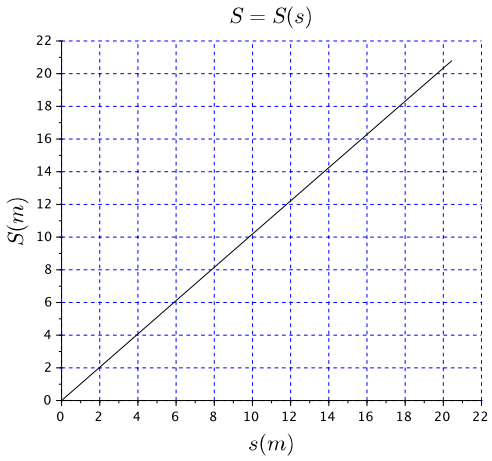

Fig. 8 Plot of $\beta = \beta(s)$

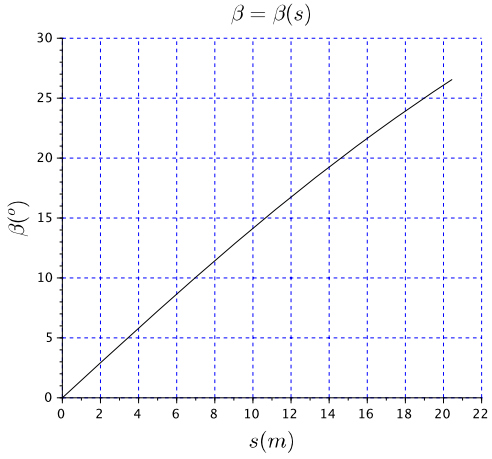

in Sect. 3.1 of this article. Thus, by applying the algorithm of Table 2, we can determine all the properties of curve C_G required by the dynamic model (Eqs. (41)–(42)).

Figures 7, 8, 9 and 10 show the plots of $S = S(s)$ (notice that $S = S(s)$ is not a straight line), $\beta = \beta(s)$, $\alpha = \alpha(s)$, and $P = P(s)$ calculated according to the algorithm of Tables 1 and 2, in the case that the curve C_G is generated from a disk of radius $R = 0.75$ m moving in contact with a concave parabola of minimum radius of curvature $P = 40$ m.

5.2 Mode switching

During the simulations, handling the two dynamic models describing the movement of the disk Eqs. (40)–(41) is a matter of utmost importance. Let us assume that the initial kinematic conditions of the disk moving in contact with the concave parabola are compatible with mode 1. As the parabola has a single minimum point and the kinetic energy of the disk gradually decreases due to friction, a unique and definitive transition to mode 2 will eventually occur after some time. Observe that this movement could be quite different if the curve, unlike a parabola, had several plateaus delimited by steep ramps as illustrated in Fig. 11.

Fig. 9 Plot of $\alpha = \alpha(s)$

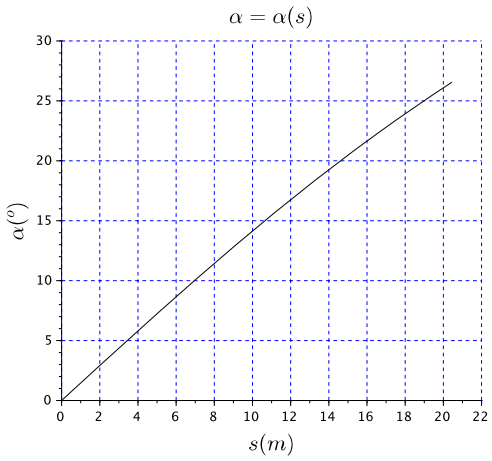

Fig. 10 Plot of $P = P(s)$

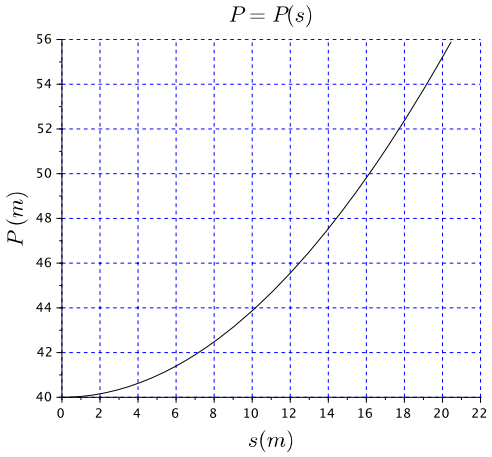

Fig. 11 Movement transitions on a curve exhibiting several plateaus

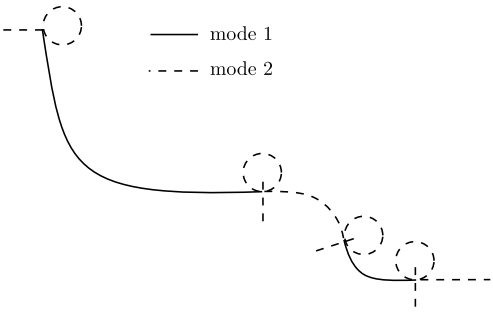

In other words, the algorithm required to control the transitions between the two modes is strongly dependent on the geometry of the curve.

Identifying the necessary and sufficient conditions for the mode switching is a crucial question. If the disk is in mode 1, it cannot switch to mode 2 unless constraint of Eq. (33)

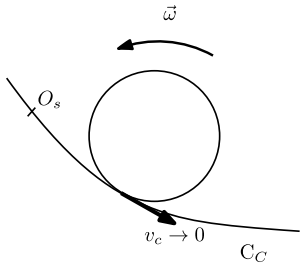

Fig. 12 Disk about to start moving in mode 2

be satisfied, *i.e.*, the point D of the disk in contact with curve C_C at time t coincides with the disk instantaneous center of rotation. However, verifying at each step of the algorithm whether this constraint came into effect or not, is not sufficient to ensure that a transition to mode 2 occurs. Let us assume, for instance, that the disk starts from rest at a point on the curve where the slope is quite steep. In such a situation, although constraint of Eq. (33) is satisfied, the disk may slide immediately after it is released if the steepness of the curve is high enough. In other words, there exists a maximum local angle slope compatible with mode 2.

To calculate this critical angle we will analyse the expression of the disk sliding acceleration. Since $\dot{S} = \dot{s} + R\dot{\theta}$, we have

$$\ddot{S} = \ddot{s} + R\ddot{\theta} = -\big[g \sin\big(\beta\big(S(s)\big)\big) + \mu\Gamma_1 \operatorname{sign}(\dot{s} + R\dot{\theta})\big] + R\ddot{\theta}. \tag{52}$$

Then, inserting Eq. (28) into Eq. (52), we obtain

$$\begin{aligned}\ddot{S} = &-\big[g \sin\big(\beta\big(S(s)\big)\big) + \mu\Gamma_1 \operatorname{sign}(\dot{s} + R\dot{\theta})\big] \\ &- \frac{m}{J_{Gz}} R\Gamma_1\big[\mu R \operatorname{sign}(\dot{s} + R\dot{\theta}) + \mu_r \operatorname{sign}(\dot{\theta})\big].\end{aligned} \tag{53}$$

Now we will consider a snapshot of the movement in which the disk, situated in a position where the slope of the curve is quite sharp, is descending the left branch of the parabola with a positive but almost null sliding velocity v_C (Fig. 12) and, consequently, with a positive but almost null angular velocity $\dot{\theta}$. The disk cannot start moving in mode 2 unless $\ddot{S} < 0$. Therefore, the maximum angle α_{crit} compatible with mode 2 is obtained from Eq. (53), admitting that

1. $\dot{s} + R\dot{\theta} > 0$ but $\dot{s} + R\dot{\theta} \to 0 \Rightarrow \operatorname{sign}(\dot{s} + R\dot{\theta}) = 1$ and $\ddot{S} \to 0$;
2. $\dot{\theta} > 0$ but $\dot{\theta} \to 0 \Rightarrow \operatorname{sign}(\dot{\theta}) = 1$ and $\ddot{\theta} \to 0$.

By imposing the above conditions on Eq. (53), we obtain

$$\left[\mu - \frac{mR}{J_{Gz}}(\mu R + \mu_r)\right] \cos\alpha_{\text{crit}}\big(S(s)\big) + \sin\beta(s) = 0, \tag{54}$$

i.e., a transcendental algebraic equation which, solved by any numerical method, gives the value of the critical angle α_{crit}.

From the above discussion we conclude that the necessary and sufficient conditions for the occurrence of a single and definitive mode 1 to mode 2 switching are: (1) the constraint Eq. (33) is satisfied; (2) the disk is in contact with a point $C(S)$ of the track for which $\alpha(S) < \alpha_{\text{crit}}$. It is important to emphasize that, in the transition from mode 1 to mode 2

the acceleration of G undergoes a sudden discontinuity, but the convergence of the sliding velocity to the null value occurs smoothly.

Now, we must verify if a switching from mode 2 to mode 1 is possible. Supposing that the disk starts the motion in mode 2, we found that, unless it reaches, at a certain instant, a point $C(S)$ of the track for which $|\alpha(S)| > |\alpha_{\text{crit}}|$, switching to mode 1 cannot occur, given that constraint of Eq. (33) is always satisfied by Eqs. (42). So, we logically might infer that a necessary condition for the disk in mode 2 to switch to mode 1 is that it starts the motion with mechanical energy E greater than a critical value given by

$$E_{\text{crit}} = mgy_G(s_{\text{crit}}) \tag{55}$$

in which $s_{\text{crit}} = s|_{\alpha(s)=\alpha_{\text{crit}}}$ is obtained from the plot of $\alpha = \alpha(s)$ and $y_G(s_{\text{crit}})$, the corresponding height y of the center G, can be calculated from Eq. (5).

The above proposition, however, leads to indeterminacy: in mode 2, constraint Eq. (33) is always satisfied, but in mode 1, the acceleration of the center of mass G, given by

$$-\left[g\sin\left(\beta\left(S(s)\right)\right) + \mu\Gamma_1 \operatorname{sign}(\dot{s} + R\dot{\theta})\right]$$

cannot be evaluated, since $\operatorname{sign}(x)$ is not defined for $x = 0$. Moreover, since the normal force $\mathbf{N}$ is always positive, there is no loss of contact with the track and, therefore, it cannot be stated that a sudden variation in the speed of contact point C, from zero to $R\dot{\theta}$ may occur.

At this point we clearly notice that, in mode 1, differential equations (41) would not properly work unless, at the transition point, the sliding velocity of the disk underwent an abrupt, discontinuous and well-known variation that, unfortunately, Coulomb's friction laws have no way of determining. Hence, we must answer the question: could such an event occur? The answer is 'yes', it actually could occur but, from the hypotheses adopted to build our dynamical model, it operates only in two modes: sliding (mode 1) and pure rolling (mode 2). For the occurrence of a sudden change in the sliding velocity of the disk, it must be assumed that it undergoes tangential collision, thus entering in mode 3 (Eqs. (31)), and returns to the track in mode 1 with a sliding velocity determined from the theory of friction collisions. This paradox was firstly identified by Painlevé [3], when he analysed the problem of a rigid homogeneous slender rod moving in contact with a flat rough surface. It can actually arise in other hybrid dynamical systems, specially those subjected to unilateral constraints and constitutive laws such as the Coulomb friction which, because of its simplicity, does not accurately describe the mechanism of contact between two non-ideal rigid bodies having rough surfaces.

Therefore, we conclude that, strictly considering all the simplified hypotheses used to build the dynamic model of Eqs. (41)–(42) of a disk moving in contact with a parabola: (1) switching from mode 2 to mode 1 is not possible (we will return to this topic in the next session, where we investigate the possibility of emulating a switching from mode 2 to mode 3 through a friction collision model); (2) as the disk cannot start the motion in mode 2 with a mechanical energy $E > E_{\text{crit}}$ without reaching an undecidable status, initial values for the generalized coordinates s and θ satisfying the constraint Eq. (33) cannot be arbitrarily chosen, but only those for which $E \leq E_{\text{crit}}$.

The previous analysis allows us to construct a simple decision making rule (Table 3) to verify, at each instant t, if a mode switching event occurs. As previously discussed, this rule does not provide the possibility of the disk undergoing free-body motion. In addition, we stress that this algorithm applies to convex functions such as the one we explore in this paper.

Table 3 Simplified rule to select the suitable mode at each step of the simulation: (a) if disk starts in mode 2 at a position where $\alpha < \alpha_{\text{crit}}$ but $E > E_{\text{crit}}$, Painlevé's paradox will eventually happen; (b) disk in mode 1 until transition to mode 2 occurs; (c) disk in mode 2 until the end of simulation; (d) disk in mode 1 until transition to mode 2 occurs

```
if ((t = 0) and (α < α_crit) and ṡ(0) = Rθ̇(0) and (E > E_crit)
    then exit; see (a)
else {
    if (|α(S(s(t)))| > α_crit)
        then do
            run Eqs. (41)
        while F = μN; see (b)
    else if (ṡ(t) + Rθ̇(t) = 0)
                then do
                    run Eqs. (42)
                until t = t_end see (c)
    otherwise
        run Eqs. (41)
    while F = μN see (d)
}
```

5.3 Initial kinematic conditions compatible with dynamics

Although $\dot{s}$ and $\dot{\theta}$ are generalized velocities (so, independent variables in phase space), this does not mean that they can be arbitrarily chosen at time $t = 0$. As pointed out by [3], the problem of identifying a compatible initial kinematic condition for a moving plane rigid body $\mathfrak{S}$ in contact with a plane fixed obstacle Σ, where dry friction forces intervene, has been previously approached by Painlevé, who discovered that an arbitrary initial kinematic imposed to $\mathfrak{S}$ can give rise either to indeterminacy or to impossibility. To avoid such impossible initial states, Delassus [5] proposed the following solution: *"to study the motion of a rigid body $\mathfrak{S}$ in contact with a fixed obstacle Σ, under the action of dry friction forces, it is necessary, in some circumstances, to make a previous study of a problem of friction collision between $\mathfrak{S}$ and Σ"*.

In order to better discuss this subject, we shall consider the schema shown in Fig. 13(a), where we see the disk connected to a cart at the instant $t = 0^-$, immediately before being put on the track. For this instant, we will suppose that: (1) the distance between G and the track is $R + \epsilon$, where ϵ is a very small distance, just sufficient to prevent the disk from touching the track at $t = 0^-$; (2) the disk has arbitrary initial kinematic conditions given by $\dot{s}_0^-$ and $\dot{\theta}_0^-$.

Figure 13(b) shows the instant at which the disk is suddenly disconnected from the cart and, due to the impulsive efforts caused by the collision with the track, assumes a new kinematic state given by $\dot{s}_0^+$ and $\dot{\theta}_0^+$.

There are numerous models proposed in the literature to physically describe the collision between two rigid bodies. In this article we will apply an approach based on the classic theory of friction collisions, originally proposed by Darboux, as stated in detail by [3] and [4]. Besides admitting that the bodies have a rigid core wrapped by a thin deformable film, the above-mentioned theory is based on five postulates [3] that permit to completely determine the new kinematic states of the bodies immediately after collision occurs. In Fig. 14, the essential elements of the friction collision between the disk and the track are presented.

The velocity of G at instant $t = 0^-$ is

$$\mathbf{v}_G^{0^-} = v_1^T \mathbf{T} + v_1^N \mathbf{N} \tag{56}$$

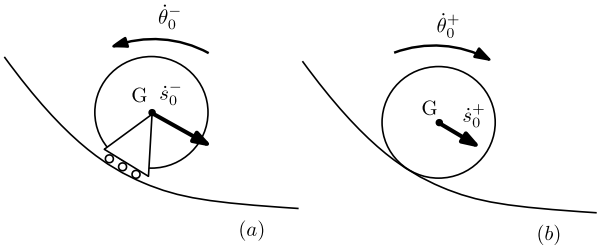

Fig. 13 Kinematic initial conditions of the disk: (**a**) immediately before touching the track; (**b**) immediately after touching the track

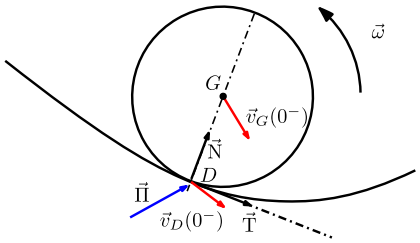

Fig. 14 Friction collision between disk and track

where v_1^T and v_1^N are the components of $\mathbf{v}_G^{0^-}$ along the axes $\mathbf{T}$ and $\mathbf{N}$, respectively. At the same instant $t = 0^-$, an unknown impulse

$$\boldsymbol{\pi} = \Pi_T \mathbf{T} + \Pi_N \mathbf{N} \tag{57}$$

is applied to the point D of the disk. From the conservation of momentum, we have

$$\begin{aligned} \Pi_T &= m\big(v_2^T - v_1^T\big), \\ \Pi_N &= m\big(v_2^N - v_1^T\big), \end{aligned} \tag{58}$$

while the conservation of angular momentum gives

$$(D - G) \wedge \boldsymbol{\pi} = m r_g^2 (\omega_2 - \omega_1)\mathbf{k} \Longrightarrow r\Pi_T = m r_g^2 (\omega_2 - \omega_1) \tag{59}$$

where r_g is the radius of gyration of the disk and $v_2^T \mathbf{T} + v_2^N \mathbf{N}$ and ω_2 are, respectively, the velocity of G and the angular velocity of the disk immediately after the collision.

This system is indeterminate, since we have only three equations (58), (59) and five unknowns $(v_2^T, v_2^N, \omega_2, \Pi_T, \Pi_N)$. Darboux's procedure to raising the problem's indeterminacy encompasses two steps: 1) postulate that the normal components of the velocities of **contact** point D, immediately before and after the collision, are related by

$$V_2 = -eV_1 \tag{60}$$

where e is the coefficient of restitution and 2) describe the motion of the body during the interval $(0^-, 0^+)$ of collision, using the equations of rigid-body dynamics,

$$\begin{aligned} m\frac{dv^T}{dt} &= F_T, \\ m\frac{dv^N}{dt} &= F_N, \\ (D-G)\wedge(F_T\mathbf{T}+F_N\mathbf{N}) &= mr_g^2\frac{d\omega}{dt}\mathbf{k} = bF_T\mathbf{k}, \end{aligned} \tag{61}$$

in which F_T and F_N, respectively, the tangential and normal components of the limited contact force between the disk and the track, depend on the tangential component U of the velocity $\mathbf{v}_D$ of the contact point D of the disk

$$\mathbf{v}_D = \mathbf{v}_G + \omega\mathbf{k}\wedge(D-G) = \big(v^T + R\omega\big)\mathbf{T} + v^N\mathbf{N}. \tag{62}$$

So far, we have seven unknowns $(v_2^T, v_2^N, \omega_2, \Pi_T, \Pi_N, F_T, F_N)$ and 7 equations to solve for them, namely, the four algebraic equations (58), (59) and (60), and the three first-order differential equations (61). Instead of integrating these last three equations, Brossard [4] analyses the graphs of the sliding velocity $\mathbf{v}$ (v^T, v^N) versus $\mathbf{F}$ (F_T, F_N) during the interval of collision, from $t = 0^-$ to $t = 0^+$. The author concludes that, for an initial sliding velocity $v_{0^-}^T = U_1 > 0$, if

$$\frac{U_1}{V_1} \geq \frac{r_g^2}{\mu(R^2+r_g^2)}(1+e) \tag{63}$$

it can be ensured [4] that v^T remains positive throughout the duration of the collision, *i.e.*, along all the $(t = 0^-, t = 0^+)$ interval. In such a case the kinematic state of the disk, as soon as it is put on the track, is given by

$$\begin{aligned} v_2^T &= v_1^T + \mu(1+e)V_1, \\ v_2^N &= v_1^N - (1+e), \\ \omega_2 &= \omega_1 + \frac{r}{r_g^2}\mu(1+e)V_1. \end{aligned} \tag{64}$$

Otherwise, in the case $v_{0^-}^T = U_1 < 0$, Eqs. (64) change to

$$\begin{aligned} v_2^T &= v_1^T - \mu(1+e)V_1, \\ v_2^N &= v_1^N - (1+e), \\ \omega_2 &= \omega_1 - \frac{r}{r_g^2}\mu(1+e)V_1. \end{aligned} \tag{65}$$

In the above equations, we must use $e = 0$, since, at instant 0^-, the distance between the surface of the disk and the track is arbitrarily small and, at instant 0^+, we suppose that the disk maintains contact with the track.

Now, we return to the controversial point discussed in the last topic. We know that, when the disk starts with $E > E_{\text{crit}}$ in mode 2 and reaches a point of the track for which $s = s_{\text{crit}}$, it actually may lose contact with the track (enter in mode 3) and, immediately, undergoes

an abrupt change in its sliding velocity (enter in mode 1). Hence, we must verify if the Darboux friction collision equations can predict such an event. Admitting that the initial sliding velocity of the disk at time 0^- is $U_1 = 0$, we found that the application of the above mentioned equations are unable to make any forecast unless the disk mass distribution is non-homogeneous and the friction coefficient is extremely low [4]. In case, for instance, coordinates of G, measured along the directions of $\mathbf{T}$ and $\mathbf{N}$ are given by $(a, b) = (R/100, R)$, and considering that the radius of gyration of a disk is $r_g = R/\sqrt{2}$, Darboux's friction collision equations provides a solution if

$$\mu < \frac{ab}{b^2 + r_g^2} = \frac{R^2/100}{3R^2/2} \approx 0.007 \tag{66}$$

Since this is not the case we are dealing with, we see that the chosen friction collision model is not suitable to detect a likely switching of the disk from mode 2 to mode 3 and then from mode 3 to mode 1. Then other friction collision models and friction laws (for instance, Contensou's friction model [10]) must be investigated in order to build a dynamical model that does not exhibit this paradox.

6 Simulation results and discussion

The motion of a disk constrained to be in permanent contact with and in the same plane as a concave parabola was simulated using the dynamical models described by the two systems of first-order differential equations (41) and (42). At each time-step of simulation, two auxiliary algorithms were used: one for calculating local geometrical properties of curves C_C and C_G (Tables 1 and 2) required for Eqs. (41) and (42) and another to select, among the two available dynamic models, the one that is compatible with the current kinematic state of the disk (Table 3). Moreover, when the disk starts from rest in mode 1, the equations provided by Darboux's friction collisions theory, like Eqs. (64)–(65), were applied to determine the correct initial kinematic conditions; if it starts in mode 2, initial kinematic state is set up in order to avoid a situation in which Painlevé's paradox occurs. The computational dynamic model was written with Scilab 5.5.1. Because the disk behaves as a non-smooth dynamic system, it was necessary to use numerical integration methods appropriate for stiff problems [18].

The values assigned to the physical and geometrical parameters of the model are given in Table 4.

A total of eight simulations for initial conditions based on s_0^-, $\dot{s}_0^-$, and $\dot{\theta}_0^-$ taken at $[-10.0, -2.0]$ m, $[-0.5, 0.5]$ m/s, and $[-15\pi, 15\pi]\, rad/s$ intervals, respectively, were performed. In Table 5 we show the corresponding initial values $\dot{s}_0^+$ and $\dot{\theta}_0^+$ calculated according to Eqs. (64)–(65). The values of the sliding velocities v_C^- immediately before the collision are also shown, in order to facilitate the analysis. Each initial condition is drawn with a different color, which will later be used in the simulation charts.

Table 4 Physical and geometric parameters adopted in the simulations

R	mass	g	p	μ	μ_r	e
m	kg	m/s^2	m	–	m	–
0.10	2.47	9.81	40.0	0.42	$0.5 \cdot 10^{-3}$	0.0

Table 5 Initial conditions immediately before and immediately after the disk is put on the track

s_0^- m	$\dot{s}_0^-$ m/s	$\dot{\theta}_0^-$ rad/s	v_C^- m/s	s_0^+ m	$\dot{s}_0^+$ m/s	s_0^+ rad/s	Line color
−10.000	−2.000	−47.124	−6.712	−10.000	−1.942	−45.965	black
−10.000	−2.000	47.124	2.712	−10.000	−2.057	45.965	blue
−10.000	−2.000	−47.124	−2.712	−10.000	2.057	−45.965	green
−10.000	−2.000	47.124	6.712	−10.000	1.942	45.965	cyan
−2.000	−2.000	−47.124	−6.712	−2.000	−1.941	−45.948	red
−2.000	−2.000	47.124	2.712	−2.000	−2.059	45.948	magenta
−2.000	−2.000	−47.124	−2.712	−2.000	2.059	−45.948	orange
−2.000	−2.000	47.124	6.712	−2.000	1.941	45.948	brown

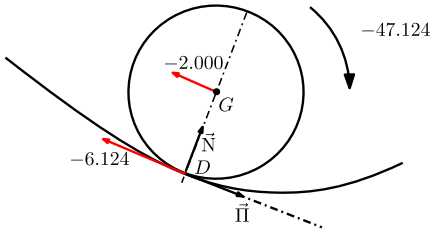

Fig. 15 Initial kinematic state of the disk when subjected to a tangential impulse

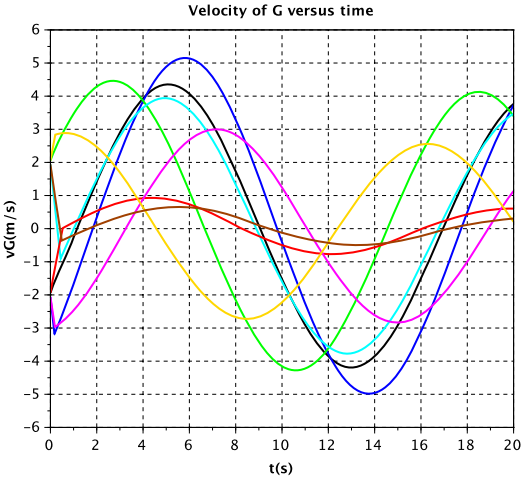

Fig. 16 Curvilinear velocity of G versus time for the initial conditions given in Table 5

Figure 15 shows the disk at an initial kinematic state $s_0^- = -10.000m/s$ and $\dot{\theta}_0^- = -47.124m/s$, when it suddenly touches the track and is submitted to a tangential impulse $\Pi_T \mathbf{T}$. Both the impulse and the corresponding impulsive moment are opposed to the directions of $\dot{s}_0^-$ and $\dot{\theta}_0^-$, respectively. As a consequence, their magnitudes diminish, as shown in Table 5 (first line).

Figures 16 and 17 show the time evolution of the state variables $\dot{s} = \dot{s}(t)$ and $\dot{\theta} = \dot{\theta}(t)$ for the initial conditions set in Table 5. In those graphs, one can identify the transition from mode 1 to mode 2: it is sufficient to observe that, around 0.3 s, the curvatures of the lines on

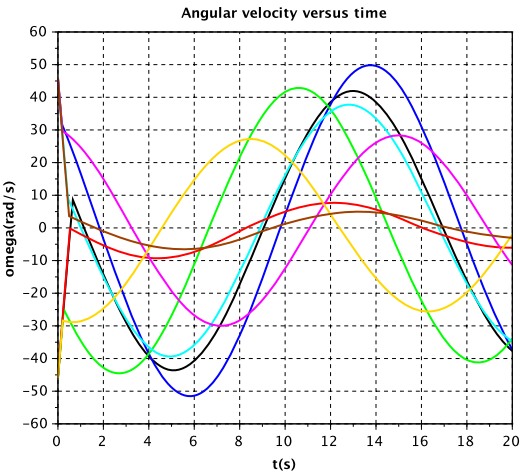

Fig. 17 Angular velocity versus time for the initial conditions given in Table 5

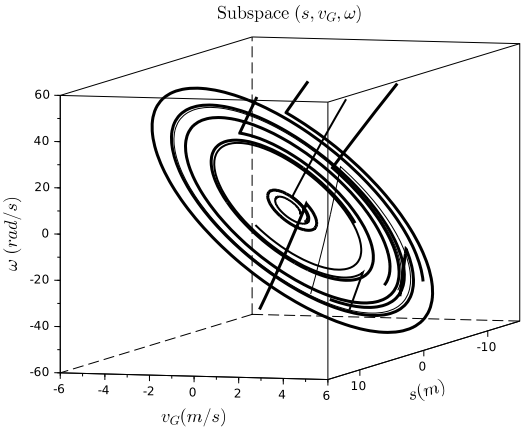

Fig. 18 Manifold $s, \dot{s}, \dot{\theta}$

the graphs undergo abrupt variations due to the sudden and discontinuous change of both $\ddot{s}$ and $\ddot{\theta}$.

Figures 18 and 19 show two manifolds of the phase space s, $\dot{s}$, θ, $\dot{\theta}$. In Fig. 18, the trajectories $s = s(\dot{s}, \dot{\theta})$ concerning mode 1, fall into distinct points of the same stable flat spiral node, characteristic of mode 2, as soon as the holonomous constraint of Eq. (33) is suddenly introduced. Starting from an initial mode 1 state, the dissipation of the kinetic energy of the disk by friction causes the disk to evolve to a kinematic state compatible with mode 2. From then on, it remains in this mode, since the parabola has a single minimum point.

In Fig. 19 we chose a three-dimensional perspective to facilitate the observation of the phase space degeneration into a diagonal plane containing curves $\dot{\theta} = \dot{\theta}(\dot{s}, \theta)$ describing mode 2. In this figure, the crossing of the phase state trajectories at the departure initial states is only apparent, since those points correspond to different values of the curvilinear abscissa s. In other words, despite the non-smoothness dynamics characteristics, the system of differential Eqs. (41)–(42) satisfy all the conditions of the Cauchy–Lipschitz theorem

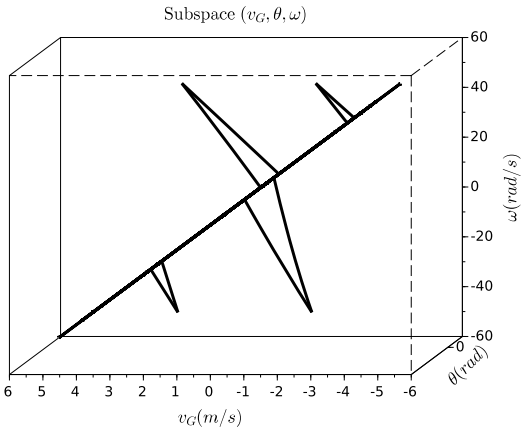

Fig. 19 Manifold $\dot{s}, \theta, \dot{\theta}$

[15]; so, for a given initial and dynamically feasible condition, there is a unique solution for those differential equations.

Many other simulations could be presented, encompassing variations in the values of the parameters of the model, like the radius R and the mass m of the disk, the minimum radius P of curvature of the track and the friction coefficients μ and μ_r. The investigation of the effects of those parameters is an important issue in nonlinear dynamics analysis, since it would allow the identification of possible bifurcation points and other interesting aspects of symplectic geometry. However, in our opinion, this would only cause the reader to get away from the vital issues discussed in this article.

7 Conclusions

In this article, the dynamic model of a disk that moves on a track described by a two-dimensional parametric curve, was thoroughly explored. Differently from the elementary cases in which the track has the form of a straight line or an arc of circumference, any other continuous two-dimensional curves introduce considerable mathematical difficulties in the modeling of the problem, forcing the use of differential geometry methods and numerical interpolation algorithms. In addition, an appropriate analysis must be made to accurately determine the instant of transition between the two modes admissible for the motion—sliding and pure rolling motion. Depending on the shape of the curve, one or more transitions between these modes may occur. Furthermore, the need for establishing initial conditions compatible with the dynamics, requires the application of the methods of a suitable friction collisions theory.

The developed model was simulated assuming that the disk moved in permanent contact with and in the same plane as a parabolic curve. Such a curve was chosen for the study because, in spite of its simple mathematical representation, it allows us to tackle the essential geometrical difficulties that must be taken into account in order to build a proper model of the disk moving in contact with a generic two-dimensional curve.

The simulations of the model, performed for distinct initial conditions – disk starting in mode 1 and evolving to mode 2, proved to be consistent with the expected dynamic behavior of the disk. Thanks to the simple shape of the track, the qualitative dynamic behavior of the disk could have been foreseen; however, coherent quantitative results can only be obtained at the expense of a considerable modeling and analysis effort.

The main drawback of the developed dynamic model concerns its inability to overcome a situation characterized by the well-known Painlevé's paradox, where the use of a simplistic Coulomb friction model and the presence of a unilateral constraint give rise to a mathematical indeterminacy. As a consequence, the model is not capable of properly simulating motions for which the disk starts in mode 2 with a mechanical energy E greater than a threshold value E_{crit}, since in such situations, an indeterminacy arises at the instant when switching from mode 2 to mode 1 would be physically necessary.

In order to generate initial kinematic states compatible with dynamics, we include the Darboux friction collision equations in our model and applied them before starting each new simulation. Unfortunately, analysis shows that Darboux's friction collision equations cannot generate a new kinematic state compatible with mode 1 if the disk is in mode 2, but on the verge to switch to model 1 as previously discussed.

We may also assert that the approach here adopted can circumvent the difficulties inherent to the focused problem and help researchers to model dynamic systems in which non-elementary geometry and non-smooth dynamics are key elements of the problem.

Important issues concerning nonlinear dynamics, such as the identification of bifurcations and other features of symplectic geometry were not approached in this paper, but are currently under investigation by our group.

Conflict of interest The authors declare that they have no conflict of interest.

References

1. Beer, F. Jr., Cornwell, E.R.: Vector Mechanics for Engineers: Dynamics, 10th edn. McGraw–Hill, New York (2012)
2. Borisov, A., Mamaev, I., Kilin, A.: Dynamics of rolling disk. Regul. Chaotic Dyn. **2**(8), 201–212 (2002)
3. Bouligand, G.: Mécanique Rationelle. Librairie Vuibert, Paris (1954)
4. Brossard, J.: Mécanique Generale, vol. 16. Institute National des Sciences Apliquées Lyon, Lyon (1994)
5. Delassus, E.: Considérations sur le frottement de glissement. In: Nouvelles Analles de Mathématiques. Bachelier, Paris (1920)
6. Doménech, A., Doménech, T., Cebrián, J.: Introduction to the study of rolling friction. Am. J. Phys. **55**, 231–235 (1987)
7. Hoscheck, J.: Offset curves in the plane. Comput. Aided Des. **2**(17), 77–82 (1985)
8. Kessler, P., O'Reilly, O.: The ringing of Euler's disk. Regul. Chaotic Dyn. **1**(7), 49–60 (2002)
9. Kunze, M.: Non-Smooth Dynamical Systems. Lecture Notes on Mathematics, vol. 1744. Springer, Berlin (1967)
10. Leine, I., Glocker, C.: A set-valued force law for spatial Coulomb–Contensou friction. Eur. J. Mech. A, Solids **22**(2), 193–216 (2003)
11. Merian, J., Kraige, L.: Engineering Mechanics: Dynamics, 8th edn. Wiley, New York (2015)
12. O'Reilly, O.: The dynamics of rolling and sliding disks. Nonlinear Dyn. **10**, 287–305 (1996)
13. Petrie, D., Hunt, J., Gray, C.: Does the euler disk slide during its motion? Am. J. Phys. **70**, 1025–1028 (2002)
14. Pham, B.: Offset curves and surfaces: a brief survey. Comput. Aided Des. **4**(24), 223–229 (1992)
15. Pontriaguine, L.: Équations Differentielles Ordinaires. Mir, Moscow (1975)
16. Przybylska, M., Rauch-Woyciechowski, S.: Dynamics of a rolling and sliding disk in a plane. Asymptotic solutions, stability and numerical simulations. Regul. Chaotic Dyn. **2**(21), 204–231 (2016)
17. Sendra, J., Winkler, F., Pérez Diaz, S.: Rational Algebraic Curves: a Computer Algebra Approach. Springer, Berlin (2007)
18. Shampine, L., Gear, C.: A user's review of solving stiff ordinary differential equations. SIAM Rev. **21**(1), 1–17 (1979)
19. Souza, D., Coluci, V.: The motion of a ball moving down a circular path. Am. J. Phys. **85**, 124–129 (2017)
20. Witter, J., Duymelinck, D.: Rolling and sliding resistive forces on balls moving on a flat surface. Am. J. Phys. **54**(80), 80–83 (1986)